NUMERICAL STUDY OF THE EFFECTS OF ICING ON VISCOUS FLOW OVER WINGS

NASA Grant NAG-3-768

Semi-Annual Progress Report

for the period

January 1 - June 30, 1993

Submitted to

NASA Lewis Research Center
Cleveland, OH 44135

Attn.: Dr. Mark Potapczuk
Icing and Cryogenics Branch

Prepared by

L. N. Sankar
Professor, School of Aerospace Engineering
Georgia Institute of Technology, Atlanta, GA 30332-0150

July 1993

INTRODUCTION

This report summarizes the progress made during the period January 1 - June 30, 1993 under the NASA Grant NAG-3-768 titled "Numerical studiy of the effects of icing on viscous flow over wings". The work was carried out by Dr. L. N. Sankar, the principal investigator, with the assistance of two graduate research assistants, Mr. Ashok Bangalore and Mr. Napporn Phaengsook. Another student, Mr. Olympio Mello, not supported under this project, also contributed to the work reported.

It may be recalled that the tasks to be performed during the current grant year are as follows:

1. Development of 3-D boundary layer methods for accurate estimates of the velocity field and surface heat transfer rates in the vicinity of the leading edge ice shape.

2. Studies of the Effects of icing on 3-D High Lift System performance

3. Continued improvement and validation of the 3-D Navier-Stokes solver

Progress was made in these areas during the reporting period. In the appendix, abstracts of two papers submitted to the AIAA 1994 Aerospace Sciences Meeting may be found. These abstracts give details of the numerical formulation and several code validation studies. Here, only an overview of the work done to date is presented.

Development of a 3-D Boundary Layer Methods: This work started out as a stand-alone 3-D steady, incompressible, boundary layer solver that will accept the surface pressure distribution from an external solver such as a panel method or a 3-D Navier-Stokes method, and will yield the velocity field and temperature field near the leading edge icing shape.

It soon became apparent to us that a stand-alone 3-D boundary layer analysis, while computationally efficient, had a number of disadvantages. Specifically,

a) 3-D boundary layer analyses break down when significant streamwise separation occurs. In the case of iced wing calculations separation can occur within the first 10% of the wing chord.

b) steady boundary layer analyses can not model unsteady effects such as shear layer instabilities, vortex shedding etc. that have been reported by other researchers.

c) The boundary layer analysis will have to be eventually coupled to an inviscid analysis, and an iterative method must be devised for full viscous-inviscid interaction. Such a fully interactive analysis can be very costly, and will break down if the wing stalls due to leading edge separation.

Of course, a 3-D Navier-Stokes analysis is very costly and is also not an acceptable way of routinely solving 3-D viscous flows.

For these reasons, an entirely new approach, based on some earlier work done by the present investigator was developed. In this approach, a two zone formulation is used. In the inner zone, the 3-D compressible Navier-Stokes equations are solved in their time dependent form. These equations do not have any singularity near the separation line, and can handle steady as well as unsteady flow phenomena. In the outer region, the 3-D unsteady compressible potential flow equation is solved. The inner and outer regions are tightly coupled to each other, so that a fully interactive analysis is achieved. There is no need to use a separate solver to specify the surface pressures, or to use viscous inviscid interaction iterations. Because the potential flow equation is solved in a fraction of the cost of the Navier-Stokes simulation, and because the Navier-Stokes zone is confined to a small region surrounding the wing, this hybrid formulation is extremely efficient, yielding results in 50% of the CPU time needed by our earlier Navier-Stokes simulations.

The abstract of a paper by Mello et al. found in the Appendix describes the hybrid procedure in detail and gives some sample results for the new formulation.

Effects of icing on 3-D High Lift System Performance: To study this problem, we are making use of a multi-block version of the Georgia Tech 3-D solver. The multi-block solver is being set up so that an arbitrary number of flaps, slats and airfoils may be used in three dimensions. The flow field is divided into a number of zones or blocks in which the flow field is advanced by one time step. The block boundary may be a solid boundary, a block interface, a far-field boundary (inflow/outflow) or a symmetry plane. We have developed a fairly general way of setting up the blocks and specifying the block interface boundary conditions.

At this writing, this solver is being debugged. We anticipate preliminary results from this solver to be available by September 1993.

Continued Development and Validation of the 3-D Navier-Stokes Solver: It may be recalled that the Georgia Tech 3-D solver does a reasonable job of predicting surface pressure distributions over iced wings. The velocity field correlations are, however, not satisfactory. In an effort to improve the velocity field predictions of the 3-D Navier-Stokes solver, during the past nine months several improvements have been made to our solver. An approximate Riemann solver replaces the central difference scheme used in the earlier versions of our code, and a k-ε turbulence model is available as an option in the solver, in addition to the Baldwin-Lomax base-line model. The appendix includes the abstract of a paper describing these enhancements, and application of this solver to iced wing configurations tested by Prof. Bragg.

APPENDIX

APPLICATION OF A THIRD ORDER UPWIND SCHEME TO VISCOUS FLOW OVER CLEAN AND ICED WINGS

A. Bangalore, N. Phaengsook and L. N. Sankar
School of Aerospace Engineering
Georgia Institute of Technology, Atlanta, GA 30332

An Abstract Presented to the

Aircraft Icing Session

32nd AIAA Aerospace Sciences Meeting, Reno,NV

SUMMARY

A 3-D compressible Navier-Stokes solver has been developed and applied to 3-D viscous flow over clean and iced wings. This method uses a third order accurate finite volume scheme with flux difference splitting to model the inviscid fluxes, and second order accurate symmetric differences to model the viscous terms. The effects of turbulence are modeled using a k-ε model. In the vicinity of the solid walls, the k and ε values are modeled using Gorski's algebraic model.

Sample results are presented for surface pressure distributions, for an untapered swept wing, made of NACA 0012 airfoil sections. The leading edge of these sections are modified using a simulated ice shape. Comparisons with the experimental data obtained by Prof. Bragg at the University of Illinois are given.

The final paper will give these results, and additional fine grid calculations now in progress.

INTRODUCTION

The aerodynamic characteristics of lifting surfaces such as wings and horizontal tails may be dramatically altered by the accumulation of ice over the leading edge. Even a relatively small amount of ice accumulation may lead to dramatic rise in pressure drag, loss in lift, and in some cases, premature stall.

Under the support of the NASA Lewis Research Center, a research effort has been underway at Georgia Tech on the effects of icing on the aerodynamic performance of lifting surfaces. Both 2-D and 3-D analyses have been developed, and calibrated [Ref. 1-3]. These analyses used relatively simple algorithms to solve the compressible Navier-Stokes equations. For example, standard second order accurate central differences are used to model the derivatives in the governing equations. A fourth order low-pass filter is used at every time step for removing any high frequency spatial oscillations. These analyses also used simple algebraic turbulence models such as the Baldwin-Lomax model to account for the effects of turbulence. Finally, for the sake of computational stability and efficiency, these methods used an implicit time-marching algorithm that permit the use of very large time steps. Reliable convergence to steady state in less than 1 CPU hour of computer time on a Cray Y/MP class of computer, on a 100,000 point grid. Reasonable correlation was observed between the calculations and the measured data obtained by Bragg and his coworkers [Ref. 4].

As these analyses were applied to a number of iced wing calculations, two drawbacks of these approaches became apparent to the present investigators. First of all, the turbulence model used in these analyses is a simple algebraic eddy viscosity model, which uses the boundary layer thickness δ^* (or an equivalent quantity such as the distance from the wall, y) as the length scale of turbulent eddies. The algebraic model used the boundary layer edge velocity U(x) (or an equivalent quantity y $|\omega|_{max}$) as a measure of the velocity scale of turbulent eddies. Such a simple representation of turbulence works well only for simple attached or mildly separated flows. In the case of iced wings, the flow field contains boundary layer over the solid surfaces, reversed flow regions, and a free shear layer coming off sharp corners and turns associated with the ice shape. The turbulent length and velocity scales for free shear layers are clearly different from the wall bounded flows. Use of a simple eddy viscosity model to such complex flows lead to inaccurate results in regions of separation. For example, the length of the separation bubble was often inaccurately predicted. Potapczuk has discussed the limitations of the Baldwin-Lomax model, and has recommended phenomenological fixes to this model [Ref. 5].

The second drawback of the previous analyses is the irrecoverable filtering out and loss of information by the low-pass filters. These filters tend to smear out shock discontinuities, contact discontinuities, and shear layers. The rate at which the filtering is applied is proportional to |u|+a , where |u| is the magnitude of local flow, and a is the speed of sound.

The present work improves upon the existing numerical analysis, presented in Ref. 3, and attempts to rectify the above two drawbacks. It uses a flux difference scheme, which dynamically and adaptively reduces the smearing of contact discontinuities, and vorticity waves, and leads to crisp resolution of free shear layers that arise in the flow. This method also uses a sophisticated k-ε model to account for the effects of turbulence. In the vicinity of solid walls, this model uses a set of phenomenologically derived boundary conditions for k and ε. The improved analysis allows transition to be detected automatically by the solver as regions of very low turbulent kinetic energy.

The improved solver has been applied to clean and iced, swept wing configurations tested by Prof. Bragg and his coworkers at the University of Illinois [Ref. 4].

The rest of this abstract is organized as follows. First, the Roe scheme is briefly outlined. Next, the k-ε formulation is described. Several sample applications of the improved solver to iced wing analysis are presented next. This abstract concludes with a list of additional results to be found in the full paper.

MATHEMATICAL AND NUMERICAL FORMULATION

The 3-D compressible Navier-Stokes equations are given in a Cartesian coordinate system as

$$\frac{\partial q}{\partial t}+\frac{\partial F}{\partial x}+\frac{\partial G}{\partial y}+\frac{\partial H}{\partial z}=\frac{\partial R}{\partial x}+\frac{\partial S}{\partial y}+\frac{\partial T}{\partial z} \qquad (1)$$

Here q is a vector of conserved flow properties; F, G and H are the inviscid flux vectors; R, S and T are viscous terms, which include the effects of turbulence through the eddy viscosity concept.

The calculations are carried out in a curvilinear body-fitted coordinate system (ξ,η,ζ). In this system, the governing equations may be written as

$$\frac{\partial \hat{q}}{\partial t}+\frac{\partial \hat{F}}{\partial \xi}+\frac{\partial \hat{G}}{\partial \eta}+\frac{\partial \hat{H}}{\partial \zeta}=\frac{\partial \hat{R}}{\partial \xi}+\frac{\partial \hat{S}}{\partial \eta}+\frac{\partial \hat{T}}{\partial \zeta} \tag{2}$$

where $\hat{q}$ etc. are related to their Cartesian counterparts by the metrics of transformation.

The Roe Scheme:

The objective of the time-marching algorithm is to advance the flow field at cells (or nodes (i,j,k) from a time level 'n' to the next time level 'n+1'. For this purpose, In the present work, equation (2) was discretized as follows:

$$\frac{\hat{q}^{n+1}_{i,j,k}-\hat{q}^{n}_{i,j,k}}{\Delta t}+\delta_\xi \overline{F}^{n+1}_{i,j,k}+\delta_\eta \overline{G}^{n+1}_{i,j,k}+\delta_\zeta \overline{H}^{n+1}_{i,j,k}=\delta_\xi \hat{R}^{n}_{i,j,k}+\delta_\eta \hat{S}^{n}_{i,j,k}+\delta_\zeta \hat{T}^{n}_{i,j,k} \tag{3}$$

where the operators δ_ξ etc. represent standard central differences such as

$$\delta_\xi \overline{F}=\frac{\overline{F}_{i+1/2}-\overline{F}_{i-1/2}}{\Delta \xi} \tag{4}$$

The numerical flux vector $\overline{F}$ differs from the physical flux vector $\hat{F}$ in a manner specified by Roe [Ref. 6]. Let q_L and q_R be two estimates to the flow field vector q , to the left side and right side of the cell face (i+1/2,j,k). Then,

$$F_{i+1/2} = \frac{\hat{F}(q_L) + \hat{F}(q_R)}{2} + \frac{1}{2} T |\Lambda| T^{-1} (q_L - q_R)$$

where,

$$q_R = q_{i+1} - \frac{q_{i+1} - q_i}{3} - \frac{q_{i+2} - q_{i+1}}{6}$$

and

$$q_L = q_i + \frac{q_{i+1} - q_i}{3} + \frac{q_i - q_{i-1}}{6}$$

(5)

Here T is a matrix that contains the left eigenvectors of the matrix $\partial \hat{F} / \partial q$, and Λ contains the eigenvalues of this matrix. These quantities must be computed using special "Roe" averages of q_L and q_R.

It may be shown that the above estimates of q_L and q_R lead to a spatially third order accurate formulation, on uniform grids and on mildly stretched grids.

Equation (3) represents a system of non-linear algebraic equations for the flow properties vector q at time level 'n+1'. Furthermore, each node (i,j+1,k) is coupled to its nine neighbors. Thus, this system of equations are highly coupled. The classical Beam-Warming approximate factorization scheme was used solve these coupled nonlinear equations, in a manner similar to that described in Reference 1.

K-e Turbulence Model

The starting point is the Boussnesq assumption for the turbulent stresses.

$$-\rho \overline{u_i u_j} = \mu_t \left(\frac{\partial u_i}{\partial x_j} + \frac{\partial u_j}{\partial x_i} \right) - \frac{2}{3} \delta_{ij} \left(\mu_t \frac{\partial u_k}{\partial x_k} + \rho k \right)$$

The turbulent viscosity μ_t has to modeled. This is achieved by modeling two physically conceivable quantities, the turbulent kinetic energy k, and the dissipation rate ε. The basic high Reynolds number K-ε model integrates the following transport equations for k and ε.

$$\rho \frac{Dk}{Dt} = \frac{\partial}{\partial X_i} \left(\frac{\mu_t}{\sigma_k} \right) \frac{\partial k}{\partial X_i} + P - \rho \varepsilon$$

$$\rho\frac{D\varepsilon}{Dt} = \frac{\partial}{\partial X_i}\left(\frac{\mu_t}{\sigma_\varepsilon}\right)\frac{\partial\varepsilon}{\partial X_i} + \frac{\varepsilon}{k}\left(C_1 P - C_2\rho\varepsilon\right)$$

The turbulent production P, is given by:

$$P = -\rho\overline{u_i u_j}\frac{\partial u_i}{\partial X_i}$$

and the turbulent viscosity μ_t is related to k and ε by :

$$\mu_t = C_\mu\rho\frac{k^2}{\varepsilon}$$

The basic k-ε model constants are as follows.

$$C_\mu = .09$$
$$C_1 = 1.43$$
$$C_2 = 1.92$$
$$\sigma_k = 1.0$$
$$\sigma_\varepsilon = 1.3$$

The k-ε Equations in Generalized Coordinates

Before the equations are discretized, they have to be transformed to the generalized ξ, η, ζ coordinate system. In this coordinate system, the k-ε equation set may be written as

$$\frac{\partial\left(\frac{k}{J}\right)}{\partial\tau} = \frac{1}{\rho}\left[\frac{\partial}{\partial\xi}\left[\frac{\mu_t}{\sigma_k}\frac{\nabla\xi\cdot\nabla\zeta}{J}k_\zeta\right] + \frac{\partial}{\partial\eta}\left[\frac{\mu_t}{\sigma_k}\frac{\nabla\eta\cdot\nabla\zeta}{J}k_\zeta\right] + \frac{\partial}{\partial\zeta}\left[\frac{\mu_t}{\sigma_k}\frac{\nabla\zeta\cdot\nabla\zeta}{J}k_\zeta\right]\right]$$
$$-\left[\frac{\partial}{\partial\xi}\left[\frac{Uk}{J}\right] + \frac{\partial}{\partial\eta}\left[\frac{Vk}{J}\right] + \frac{\partial}{\partial\zeta}\left[\frac{Wk}{J}\right]\right] + \frac{P}{\rho J} - \frac{\varepsilon}{J}$$

$$\frac{\partial\left(\frac{\varepsilon}{J}\right)}{\partial\tau} = \frac{1}{\rho}\left[\frac{\partial}{\partial\xi}\left[\frac{\mu_t}{\sigma_\varepsilon}\frac{\nabla\xi\cdot\nabla\zeta}{J}\varepsilon_\zeta\right] + \frac{\partial}{\partial\eta}\left[\frac{\mu_t}{\sigma_\varepsilon}\frac{\nabla\eta\cdot\nabla\zeta}{J}\varepsilon_\zeta\right] + \frac{\partial}{\partial\zeta}\left[\frac{\mu_t}{\sigma_k}\frac{\nabla\zeta\cdot\nabla\zeta}{J}\varepsilon_\zeta\right]\right]$$
$$-\left[\frac{\partial}{\partial\xi}\left[\frac{U\varepsilon}{J}\right] + \frac{\partial}{\partial\eta}\left[\frac{V\varepsilon}{J}\right] + \frac{\partial}{\partial\zeta}\left[\frac{W\varepsilon}{J}\right]\right] + \frac{\varepsilon}{k}\left(C_1\frac{P}{\rho J} - C_2\frac{\varepsilon}{J}\right)$$

Here U,V,W art the contravariant components of velocity and J is the Jacobian.

In expanding the equations one reasonable assumption is made. In the diffusion terms, only the gradient of the quantities k and ε in the ζ direction are kept, the variation in the ξ and η directions are neglected. This is justifiable as the maximum changes in the turbulent quantities occur only across the shear layer. The production term P is given by,

$$P = \frac{C_\mu k^2 \hat{P}}{J\varepsilon}$$

$$\hat{P} = \left(2\cdot\frac{\partial u}{\partial x}\right)\frac{\partial u}{\partial x} + \left(\frac{\partial u}{\partial y} + \frac{\partial v}{\partial x}\right)\frac{\partial u}{\partial y} + \left(\frac{\partial u}{\partial z} + \frac{\partial w}{\partial x}\right)\frac{\partial u}{\partial z} +$$
$$\left(\frac{\partial v}{\partial x} + \frac{\partial u}{\partial y}\right)\frac{\partial v}{\partial x} + \left(2\cdot\frac{\partial v}{\partial y}\right)\frac{\partial v}{\partial y} + \left(\frac{\partial v}{\partial z} + \frac{\partial w}{\partial y}\right)\frac{\partial v}{\partial z} +$$
$$\left(\frac{\partial w}{\partial x} + \frac{\partial u}{\partial z}\right)\frac{\partial w}{\partial x} + \left(\frac{\partial w}{\partial y} + \frac{\partial v}{\partial z}\right)\frac{\partial w}{\partial z} + \left(2\cdot\frac{\partial w}{\partial z}\right)\frac{\partial w}{\partial z}$$

The various derivatives with respect to x, y and z may be computed in terms of the generalized coordinates as follows,

$$\frac{\partial}{\partial x} = \xi_x\frac{\partial}{\partial\xi} + \eta_x\frac{\partial}{\partial\eta} + \zeta_x\frac{\partial}{\partial\zeta}$$
$$\frac{\partial}{\partial y} = \xi_y\frac{\partial}{\partial\xi} + \eta_y\frac{\partial}{\partial\eta} + \zeta_y\frac{\partial}{\partial\zeta}$$
$$\frac{\partial}{\partial z} = \xi_z\frac{\partial}{\partial\xi} + \eta_z\frac{\partial}{\partial\eta} + \zeta_z\frac{\partial}{\partial\zeta}$$

The goal of the k-ε solver is to compute k and ε at a time level 'n+1', given these values at time level 'n'. In this formulation the "right hand side residual" is first calculated for the whole region .

RHS = Diffusion - Convection + Production - Dissipation

The convection terms were computed using two-point upwind schemes, as follows:

$$\frac{U}{J}\frac{\partial k}{\partial \xi} \cong \frac{U}{J}\tilde{\delta}_{\xi}k = \frac{U+|U|}{2J\Delta\xi}(k_i - k_{i-1}) + \frac{U-|U|}{2J\Delta\xi}(k_{i+1} - k_i)$$

The diffusion terms were computed using central differences as follows:

$$\frac{\partial}{\partial\xi}\left[\frac{\mu_t}{\sigma_\varepsilon}\frac{\nabla\xi\cdot\nabla\zeta}{J}k_\zeta\right] = \frac{1}{\Delta\xi}\left(\frac{1}{\sigma_k}\left((\mu_t)_{i+1/2}\cdot\left(\frac{\nabla\xi\cdot\nabla\zeta}{J}\right)_{i+1/2}\cdot(k_\zeta)_{i+1/2}\right) - \left((\mu_t)_{i-1/2}\cdot\left(\frac{\nabla\xi\cdot\nabla\zeta}{J}\right)_{i-1/2}\cdot(k_\zeta)_{i-1/2}\right)\right)$$

$$\frac{\partial}{\partial\eta}\left[\frac{\mu_t}{\sigma_\varepsilon}\frac{\nabla\eta\cdot\nabla\zeta}{J}k_\zeta\right] = \frac{1}{\Delta\eta}\left(\frac{1}{\sigma_k}\left((\mu_t)_{j+1/2}\cdot\left(\frac{\nabla\eta\cdot\nabla\zeta}{J}\right)_{j+1/2}\cdot(k_\zeta)_{j+1/2}\right) - \left((\mu_t)_{j-1/2}\cdot\left(\frac{\nabla\eta\cdot\nabla\zeta}{J}\right)_{j-1/2}\cdot(k_\zeta)_{j-1/2}\right)\right)$$

$$\frac{\partial}{\partial\zeta}\left[\frac{\mu_t}{\sigma_k}\frac{\nabla\zeta\cdot\nabla\zeta}{J}k_\zeta\right] = \frac{1}{\Delta\zeta}\left(\frac{1}{\sigma_k}\left((\mu_t)_{k+1/2}\cdot\left(\frac{\nabla\zeta\cdot\nabla\zeta}{J}\right)_{k+1/2}\cdot(k_\zeta)_{k+1/2}\right) - \left((\mu_t)_{k-1/2}\cdot\left(\frac{\nabla\zeta\cdot\nabla\zeta}{J}\right)_{k-1/2}\cdot(k_\zeta)_{k-1/2}\right)\right)$$

After the right hand side is computed, an approximate factorization scheme is used here to solve for the changes in k and ε from tone time step. This requires the solution of the following matrix product equation.

$$\left[1+U\Delta t\bar{\delta}_{\xi}\right]\left[1+V\Delta t\bar{\delta}_{\eta}\right]\left[1+W\Delta t\bar{\delta}_{\zeta}\right]\begin{Bmatrix}k^{n+1}-k^{n}\\ \varepsilon^{n+1}-\varepsilon^{n}\end{Bmatrix}=J\Delta t(RHS)^{n}$$

Each of the three matrices (or operators) are invertible.

To start the calculations, the k and ε fields were initialized to small non-zero positive values. Near solid walls, the classical high Reynolds number k-e model breaks down. In the present work, near the solid wall, the k and ε were assumed to have the following variation:

$$k = A\, y^3$$

$$\varepsilon = \text{constant}$$

RESULTS AND DISCUSSION

Navier-Stokes calculations were carried out using the flow solver developed in the previous section, for a swept untapered wing tested by Bragg et al. The airfoil sections are made of NACA 0012 airfoil sections. The wing tested had a chord length of 15 inches and a semispan of 37.25 inches. To study the effects of icing, the leading edge was modified with a simulated ice shape. This ice shape corresponds to that measured at the NASA Lewis Icing Research Tunnel. for a NACA 0012 airfoil, at a freestream velocity of 130 mph, angle of attack of 4 degrees, icing time of 4 minutes, volume median droplet diameter of 20 microns, liquid water content of 2.1 grams per cubic meter and a temperature of 18 degrees. Bragg's measurements were done at zero sweep and at a 30 degree sweep.

The calculations used a 121 x 24 x 45 grid, with 91 points on the airfoil at each span station, 14 spanwise stations over the wing, and 45 points in the direction normal to the wing surface. Roughly a quarter of these points are in the boundary layer region. Thus, the boundary layer is only moderately resolved in these preliminary calculations.

Figure 1 shows the surface pressure distribution for the clean wing at 8 degrees angle of attack at 5 spanwise locations: 27%, 42%, 56%, 72% and 89%. In general, the comparisons are in good agreement with the measured data. The suction peak near the leading edge, and the rapid compression of the flow over the upper surface were well predicted. No angle of attack corrections to account for the effects of the wind tunnel blockage were made. The flow solver had no user adjustable constants, and was run using the standard k-ε constants described in the previous sections.

Figure 2 shows the calculations and measurements for the iced wing. In this case, the flow separates over the leading edge ice shape, and forms a plateau. The Roe k-ε is seen to perform satisfactorily at the inboard stations. Near the wing tip, the agreement is poor. At this writing, we are repeating this particular analysis with a clustered grid near the tip region to see if an improved resolution of the tip vortex will lead to an improved prediction of the surface pressures at the outboard station.

Figure 3 shows some preliminary results for the velocity field at selected spanwise and chordwise locations, for the iced swept wing. Both the k-ε results and the original algebraic model results are shown. The computed qualities plotted are the u- component (chordwise) of velocity, while the measured data are tangential to to the airfoil/wing surface. As a result, a discrepancy exists at the boundary layer edge.

ADDITIONAL RESULTS TO BE PRESENTED IN THE FULL PAPER

a) The full paper will contain results for the swept wing considered above and the unswept wing, on a denser grid. We are increasing the number of nodes in the boundary layer region, and in the spanwise direction, particularly near the tip. The final paper will contain these fine grid calculations.

b) A wealth of LDV data is available in the Ph. D. dissertation of Khodadoust [Ref. 7]. The computed velocity profile at selected stations over the clean and iced wing will be compared with the measured data in the full paper.

CONCLUDING REMARKS

An existing compressible Navier-Stokes solver for clean and iced wing analysis has been upgraded through the use of state of the art upwind difference schemes, and a two equation k-ε model. Encouraging preliminary results have been obtained for swept, clean and iced wing configurations. The additional overhead associated with the Roe scheme and the k-e model has been partially offset by improvements to the algorithm elsewhere. A careful systematic validation of the improved flow solver is now underway, prior to its adaptation for iced wing performance analysis.

REFERENCES

1. Wu, Jiunn-Chi, "A Study of Unsteady Turbulent Flow past Airfoils," Ph. D. Dissertation, Georgia Institute of Technology, Atlanta, GA 1988.

2. Kwon, O. J., and Sankar, L. N., "Numerical Study of the Effects of Icing on Finite Wing Aerodynamics," AIAA Paper 90-0757.

3. Kwon, O. J. and Sankar, L. N., "Numerical Study of the Effects of icing on Fixed and Rotary Wing Aerodynamics," AIAA paper 91-0662.

4. Bragg, M. B. and Khodadoust, A., "Effects of Simulated Glaze Ice on a Rectangular Wing," AIAA paper 89-0750.

5. Potapczuk, M., "Navier-Stokes Analysis of Airfoils with Leading Edge Ice Accretions," Ph. D. Dissertation, The University of Akron, Akron, Ohio, 1989.

6. Roe, P. L., "Approximate Riemann Solvers, Parameter Vectors and Difference Schemes," Journal of Computational Physics, Vol. 43, 1981, pp 357-372.

7. Khodadoust, A., "An Experimental Study of the Flow Field on a Semi-Span Wing with a Simulated Glaze Ice Accretion," Ph. D. Dissertation, University of Illinois at Urbana-Champaign, 1993.

Figure 1a

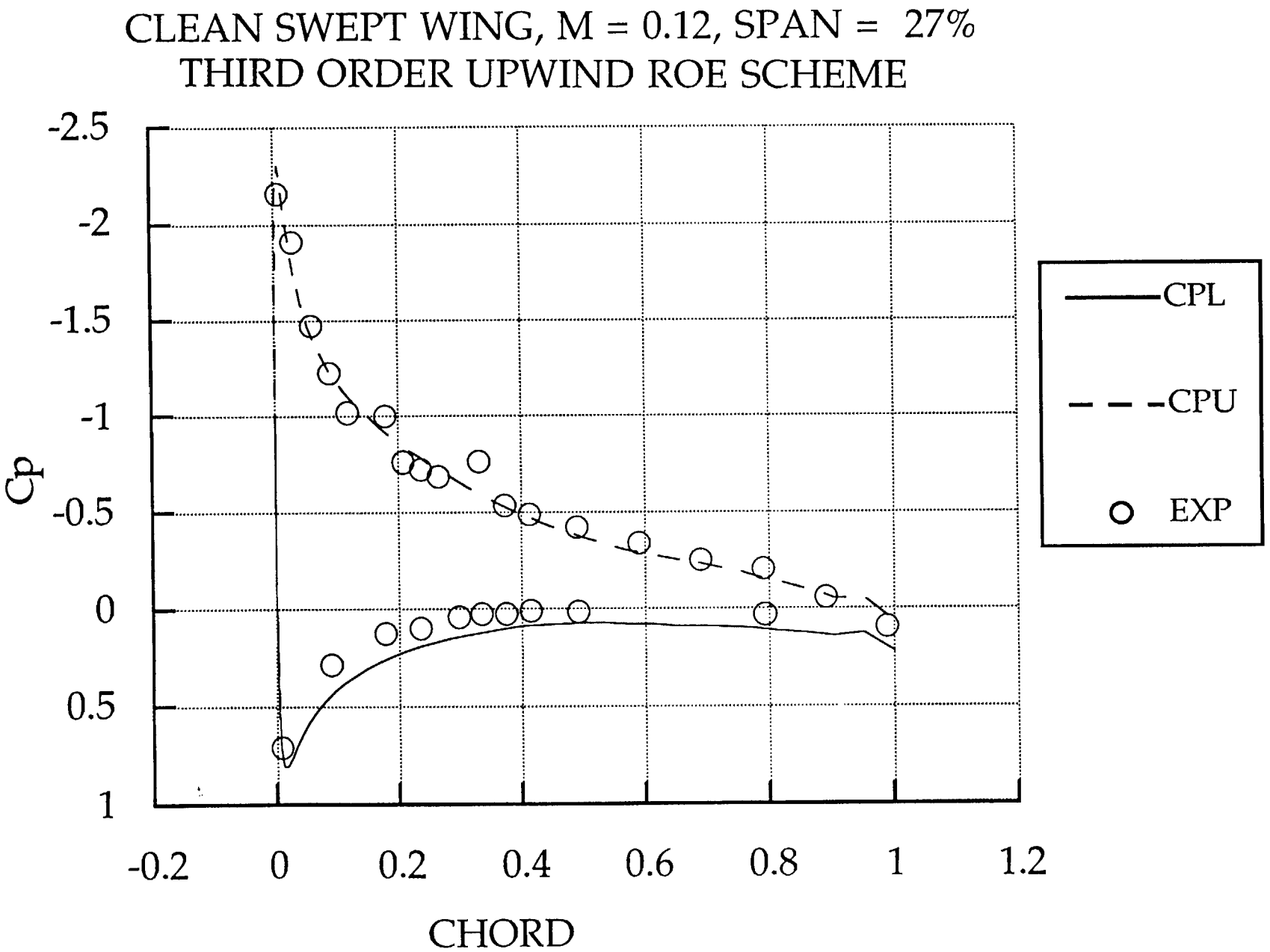
CLEAN SWEPT WING, M = 0.12, SPAN = 27%
THIRD ORDER UPWIND ROE SCHEME
-2.5
-2
-1.5
-1
-0.5
0
0.5
1
Cp
-0.2
0
0.2
0.4
0.6
0.8
1
1.2
CHORD
CPL
CPU
EXP

Figure 2b

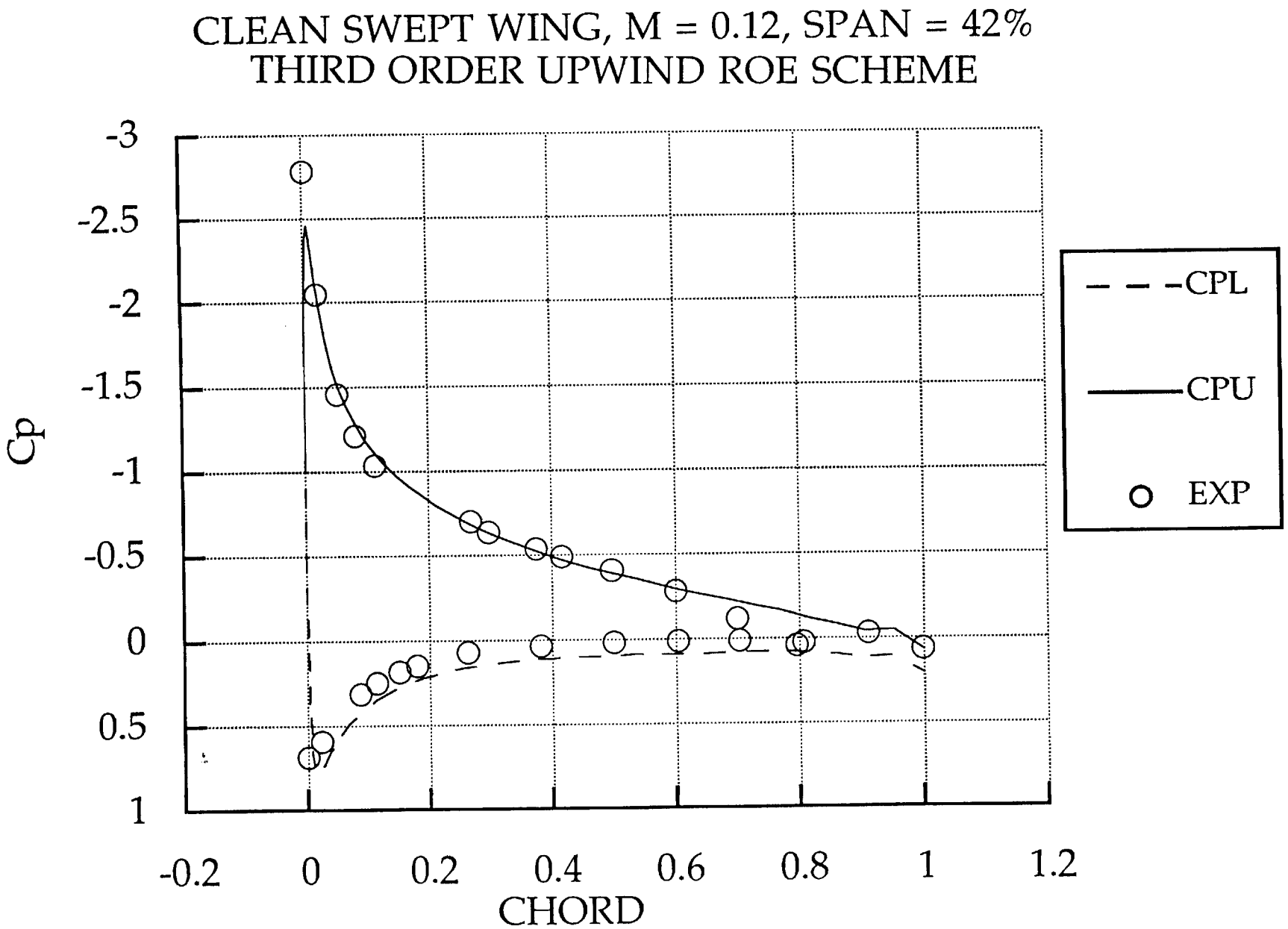
CLEAN SWEPT WING, M = 0.12, SPAN = 42%
THIRD ORDER UPWIND ROE SCHEME
Cp
-3
-2.5
-2
-1.5
-1
-0.5
0
0.5
1
-0.2
0
0.2
0.4
0.6
0.8
1
1.2
CHORD
CPL
CPU
EXP

Figure 1c

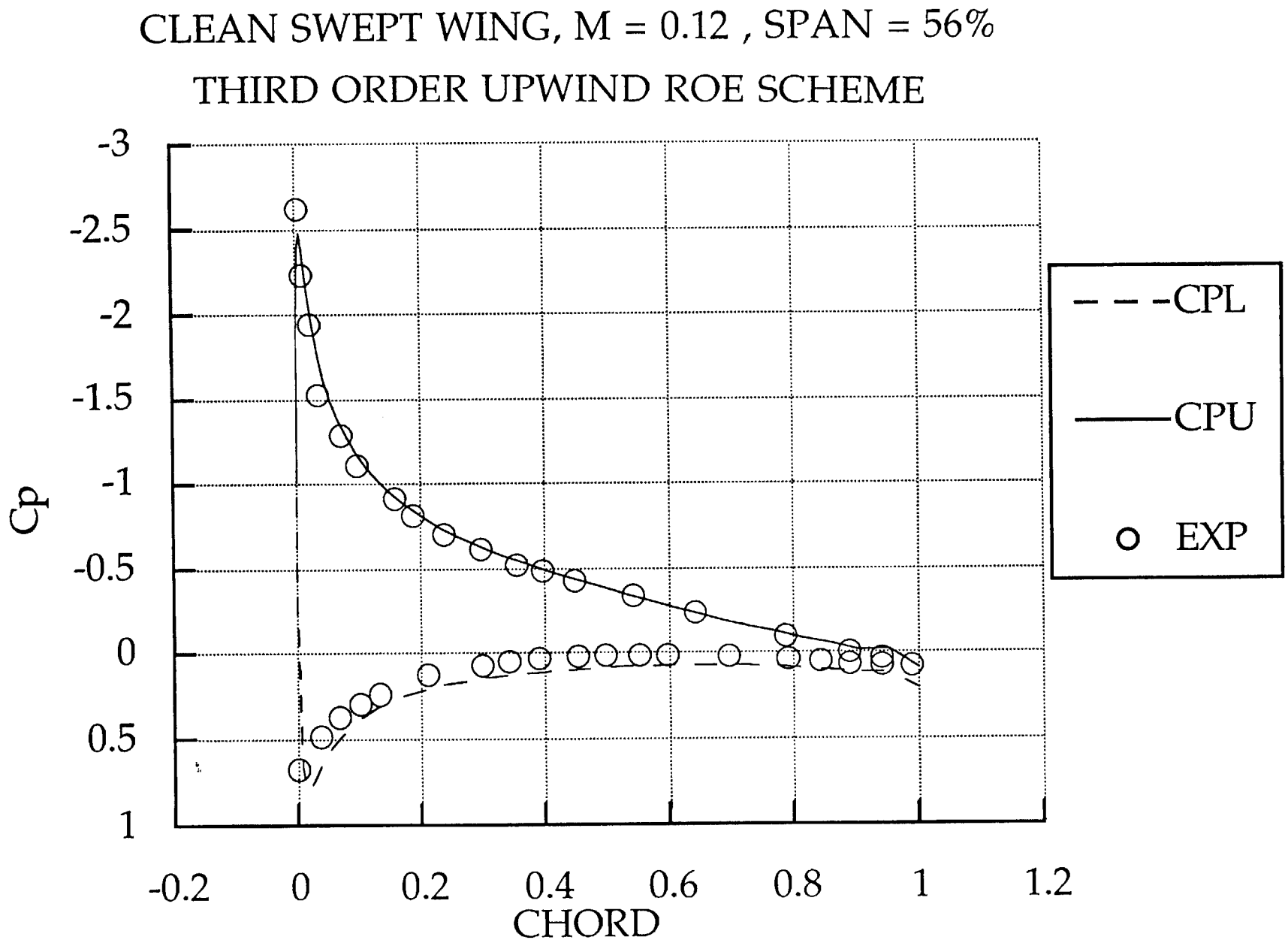
CLEAN SWEPT WING, M = 0.12 , SPAN = 56%
THIRD ORDER UPWIND ROE SCHEME
Cp
-3
-2.5
-2
-1.5
-1
-0.5
0
0.5
1
-0.2
0
0.2
0.4
0.6
0.8
1
1.2
CHORD
CPL
CPU
EXP

Figure 1 d

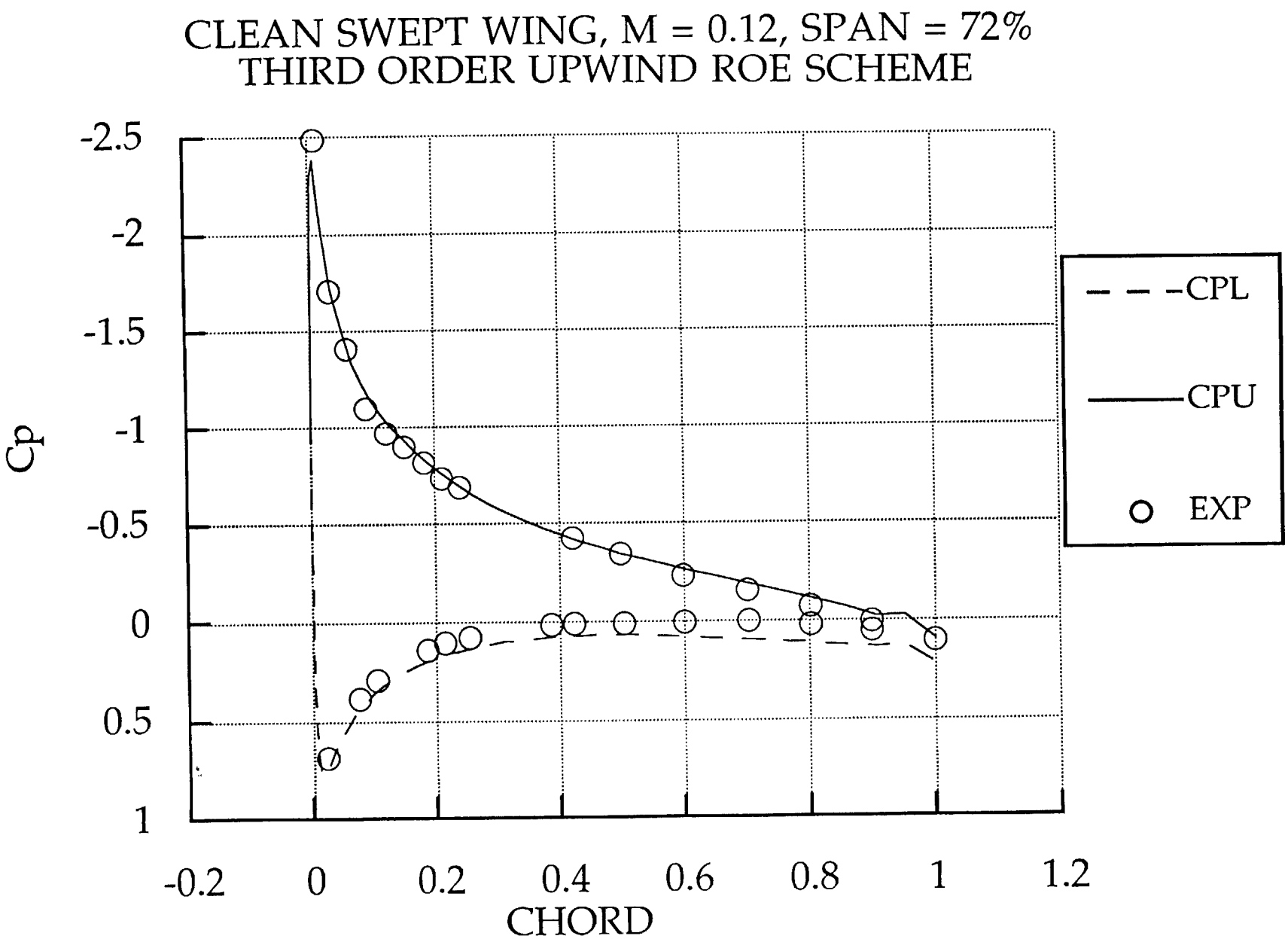
CLEAN SWEPT WING, M = 0.12, SPAN = 72%
THIRD ORDER UPWIND ROE SCHEME
Cp
-2.5
-2
-1.5
-1
-0.5
0
0.5
1
-0.2
0
0.2
0.4
0.6
0.8
1
1.2
CHORD
CPL
CPU
EXP

Figure 1e

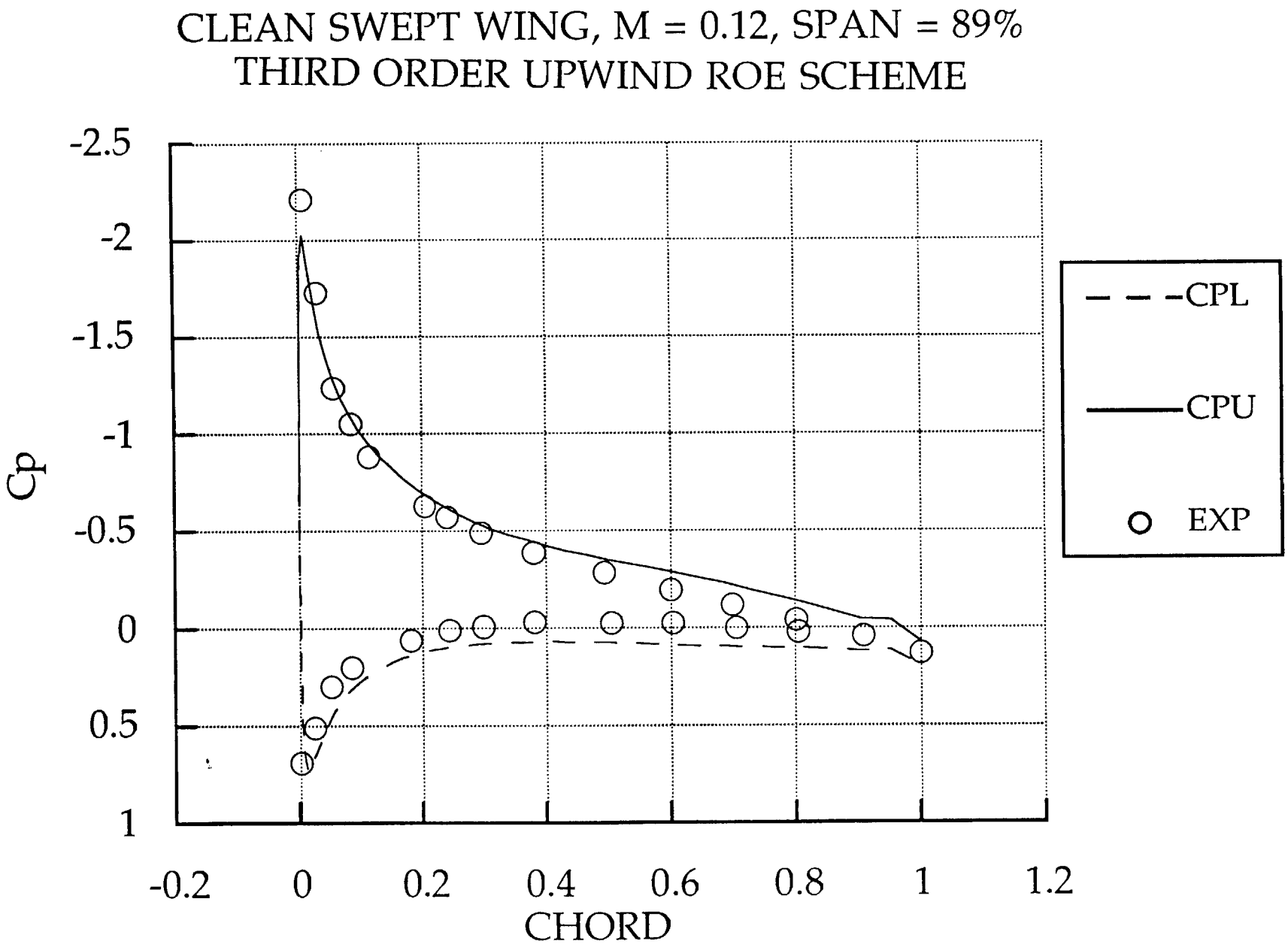
CLEAN SWEPT WING, M = 0.12, SPAN = 89%
THIRD ORDER UPWIND ROE SCHEME
-2.5
-2
-1.5
-1
-0.5
0
0.5
1
Cp
-0.2
0
0.2
0.4
0.6
0.8
1
1.2
CHORD
CPL
CPU
EXP

Figure 2a

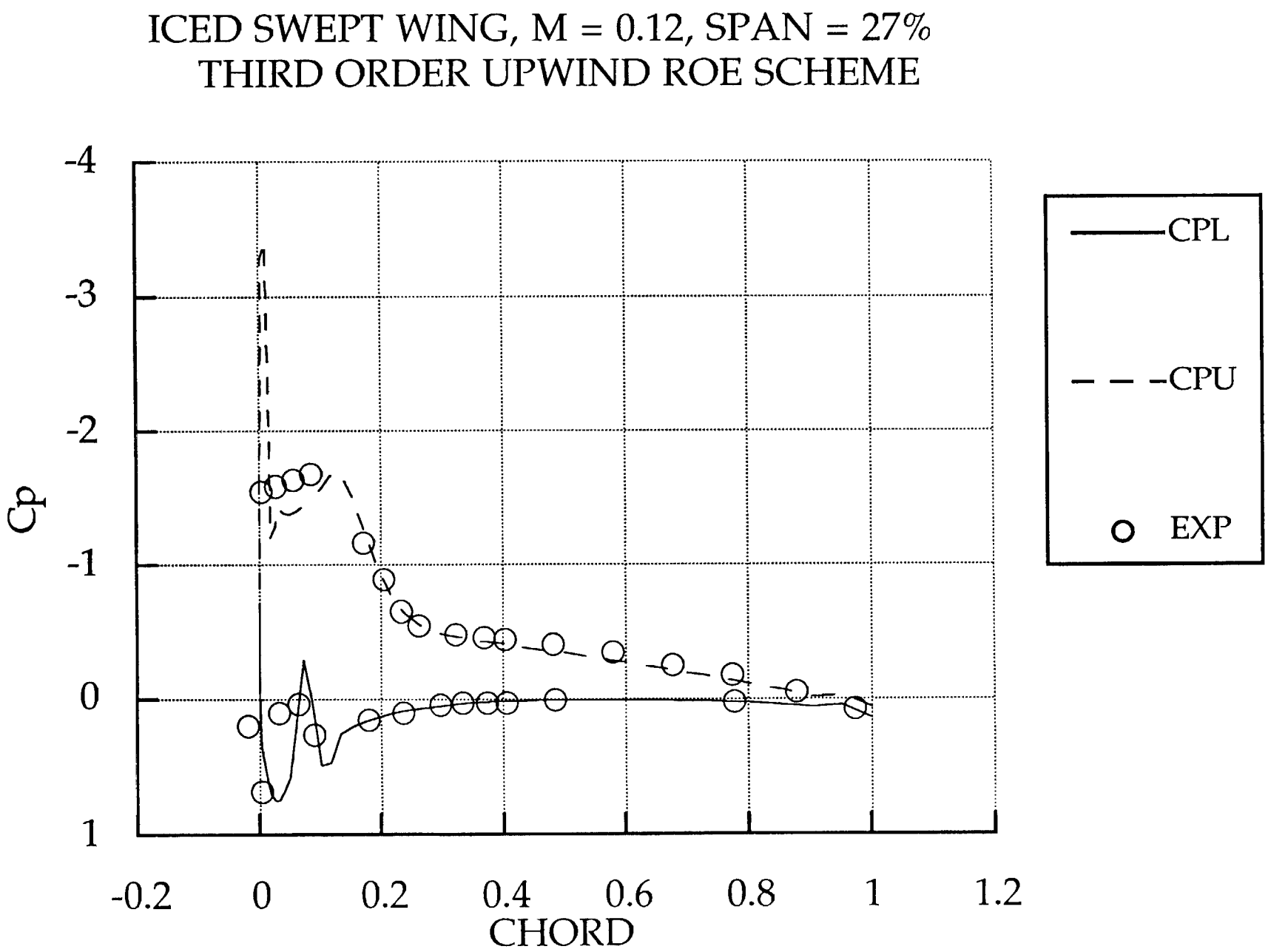
ICED SWEPT WING, M = 0.12, SPAN = 27%
THIRD ORDER UPWIND ROE SCHEME
-4
-3
-2
-1
0
1
Cp
-0.2
0
0.2
0.4
0.6
0.8
1
1.2
CHORD
CPL
CPU
EXP

Figure 2b

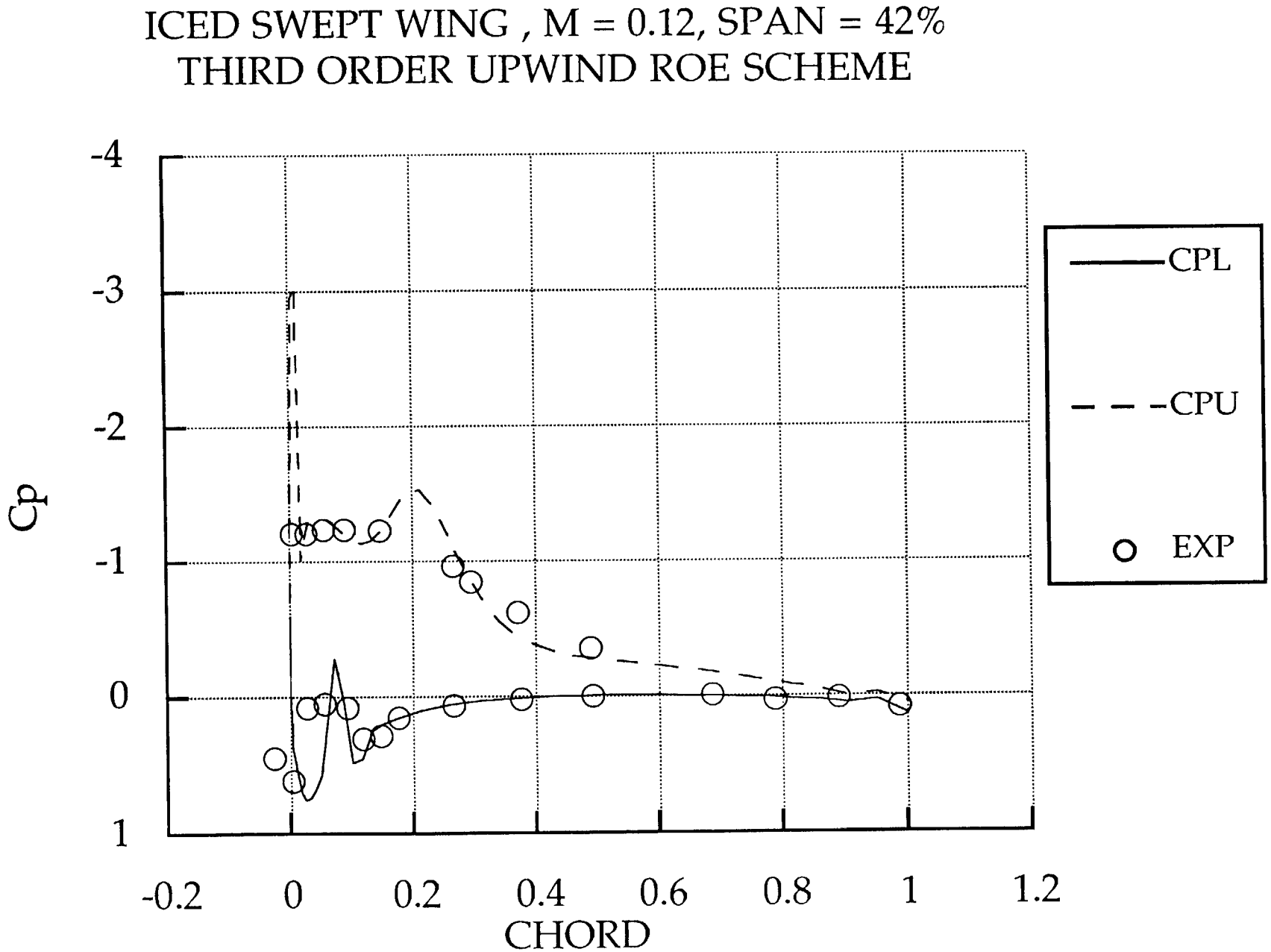
ICED SWEPT WING , M = 0.12, SPAN = 42%
THIRD ORDER UPWIND ROE SCHEME
Cp
-4
-3
-2
-1
0
1
-0.2
0
0.2
0.4
0.6
0.8
1
1.2
CHORD
CPL
CPU
EXP

Figure 2C

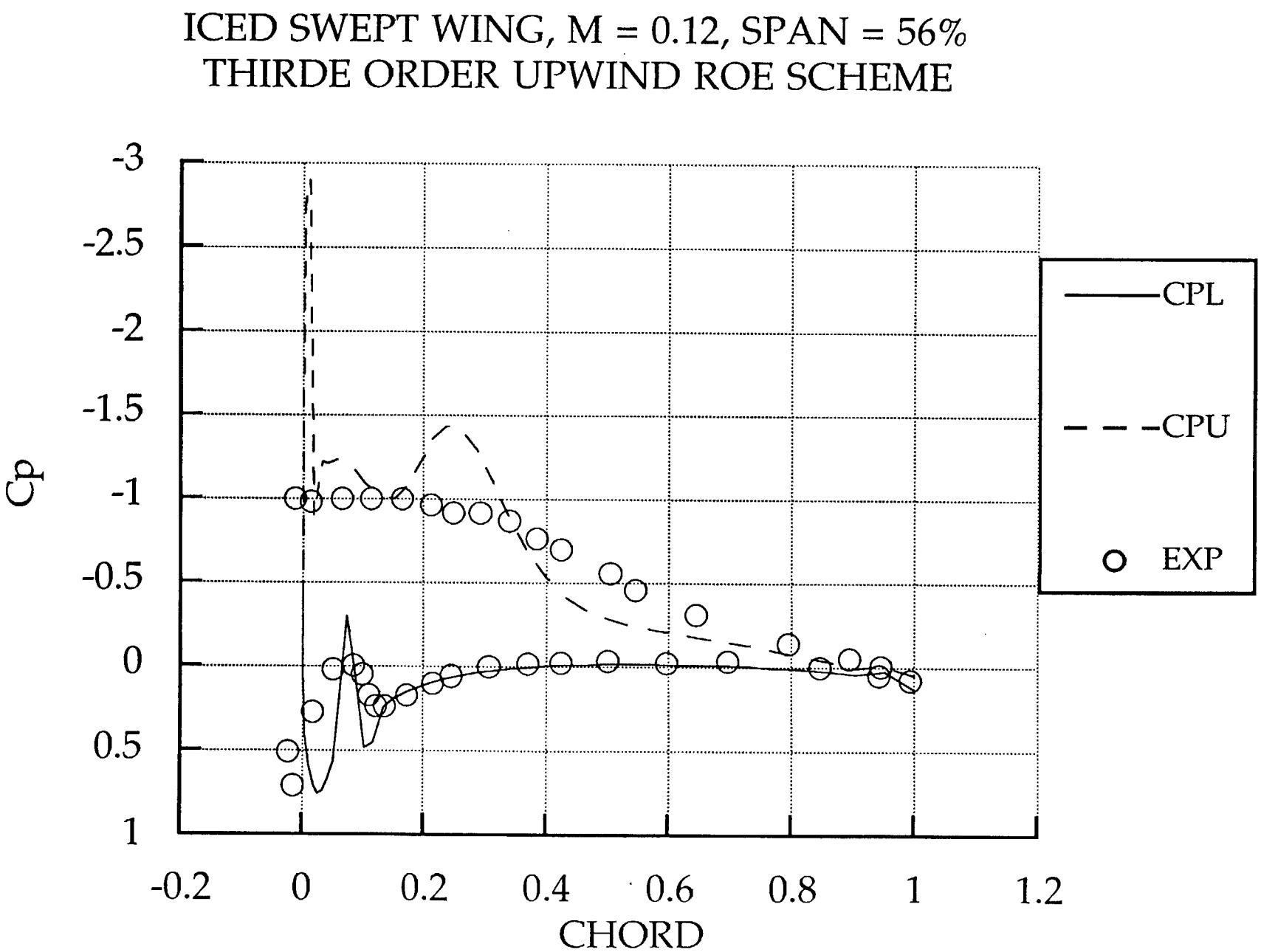
ICED SWEPT WING, M = 0.12, SPAN = 56%
THIRDE ORDER UPWIND ROE SCHEME
Cp
-3
-2.5
-2
-1.5
-1
-0.5
0
0.5
1
-0.2
0
0.2
0.4
0.6
0.8
1
1.2
CHORD
CPL
CPU
EXP

Figure 2d

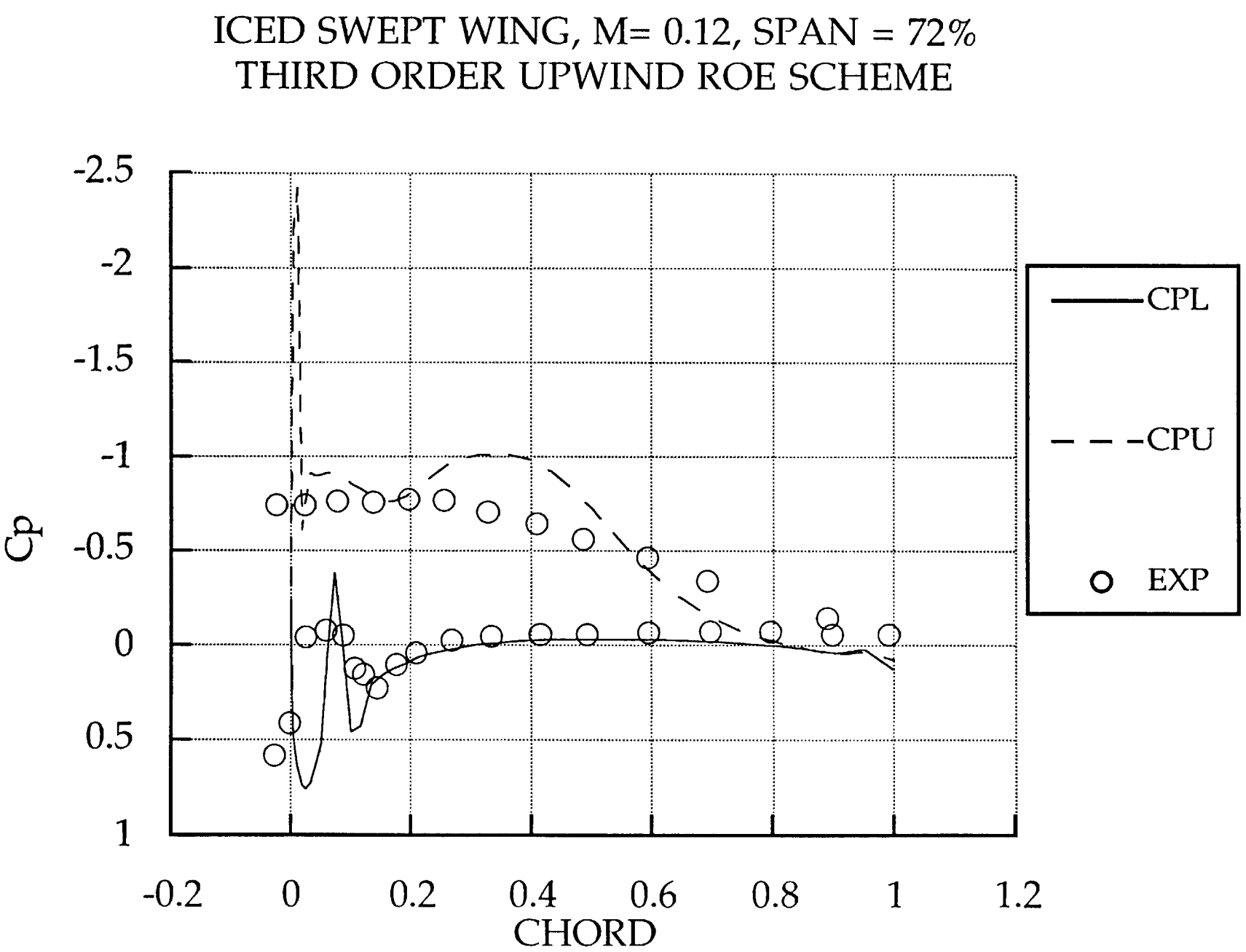
ICED SWEPT WING, M= 0.12, SPAN = 72%
THIRD ORDER UPWIND ROE SCHEME
-2.5
-2
-1.5
-1
-0.5
0
0.5
1
Cp
-0.2
0
0.2
0.4
0.6
0.8
1
1.2
CHORD
CPL
CPU
EXP

Figure 2e

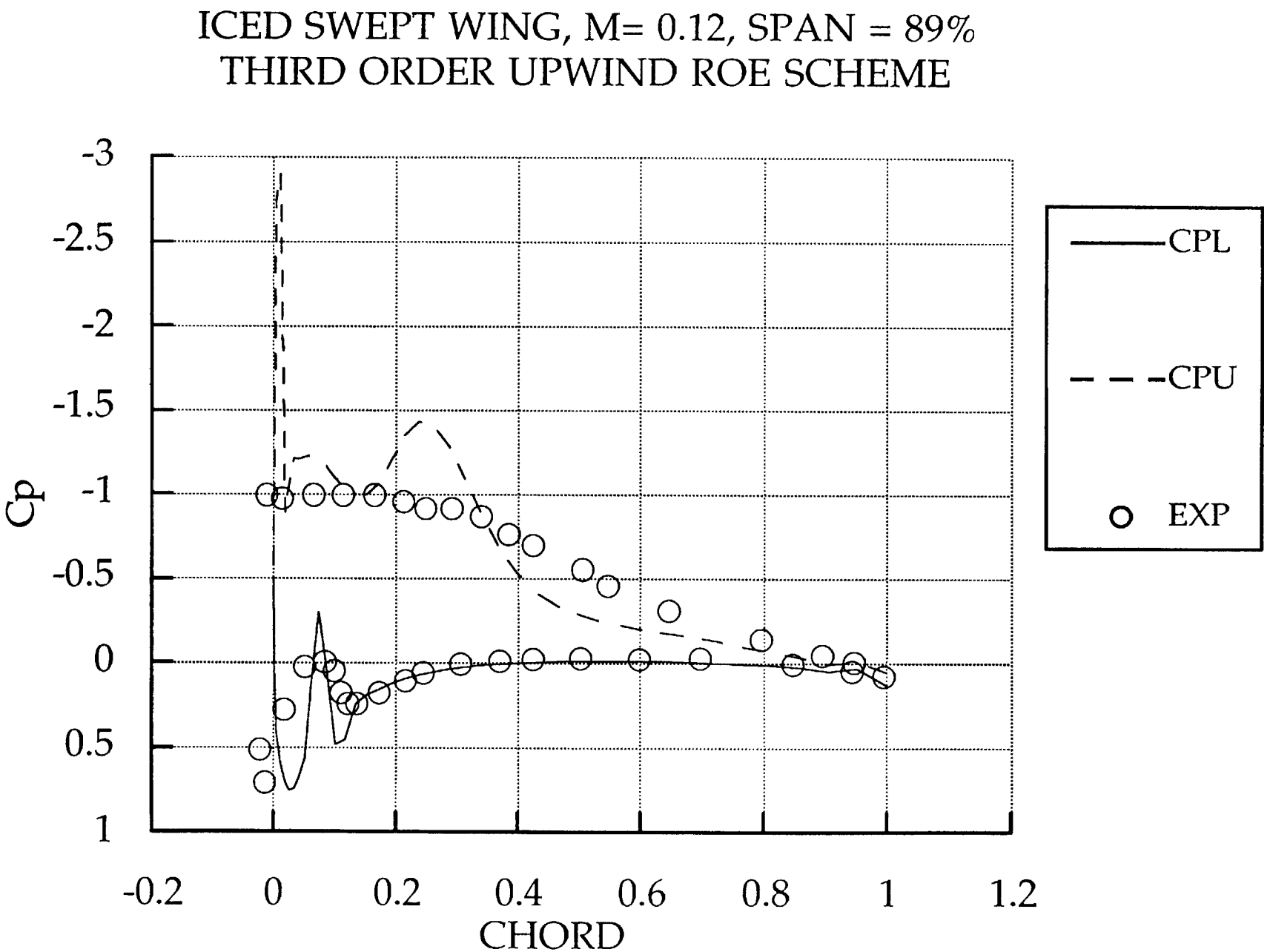
ICED SWEPT WING, M= 0.12, SPAN = 89%
THIRD ORDER UPWIND ROE SCHEME
Cp
-3
-2.5
-2
-1.5
-1
-0.5
0
0.5
1
-0.2
0
0.2
0.4
0.6
0.8
1
1.2
CHORD
CPL
CPU
EXP

Figure 3a

BOUNDARY LAYER STREAMWISE VELOCITY PROFILE
NACA 0012 ICED SWEPT WING, x/c = 0.30, y/b = 0.6

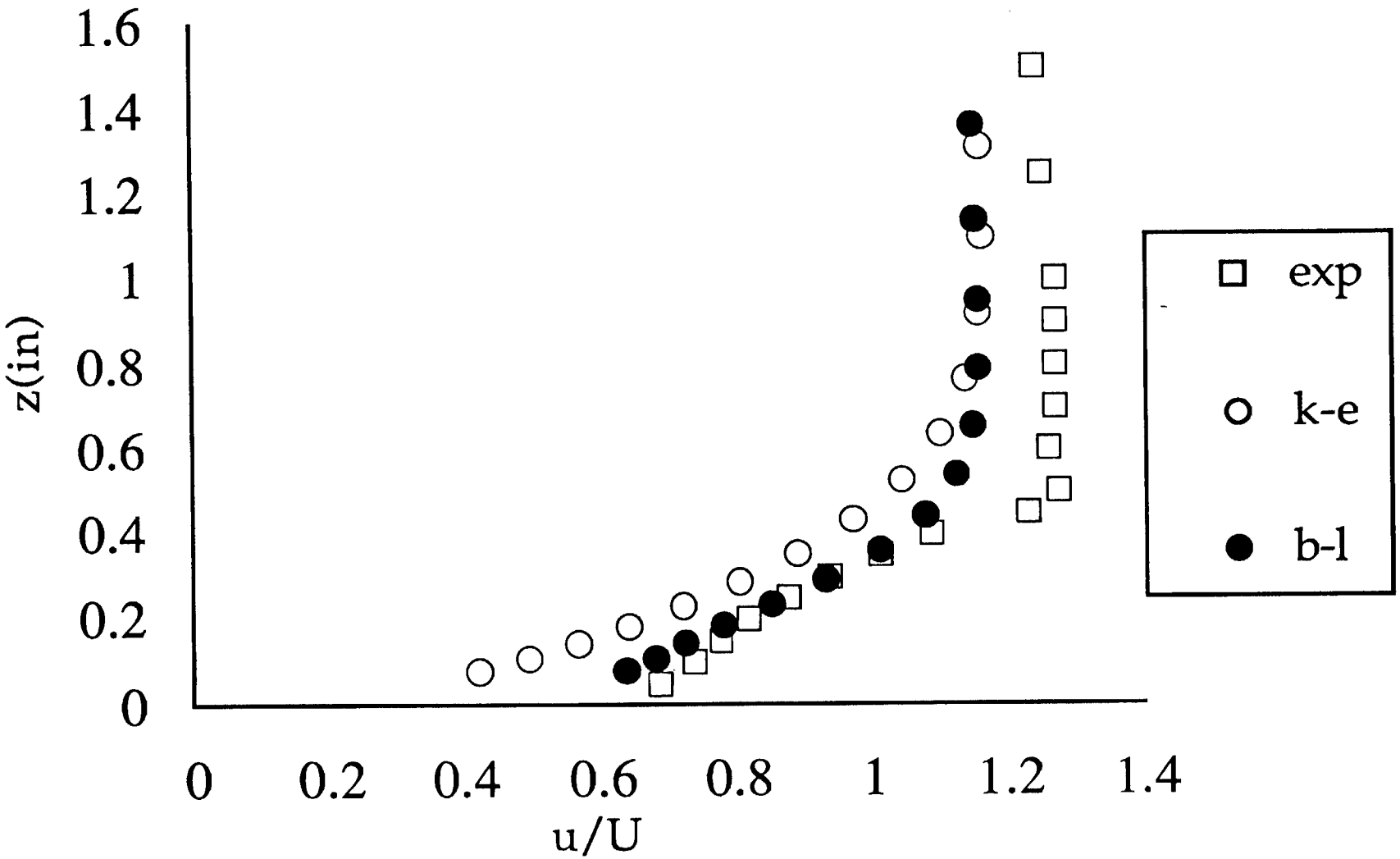

Figure 3b

BOUNDARY LAYER STREAMWISE VELOCITY PROFILE
NACA 0012 ICED SWEPT WING, x/c = 0.18, y/b = 0.6

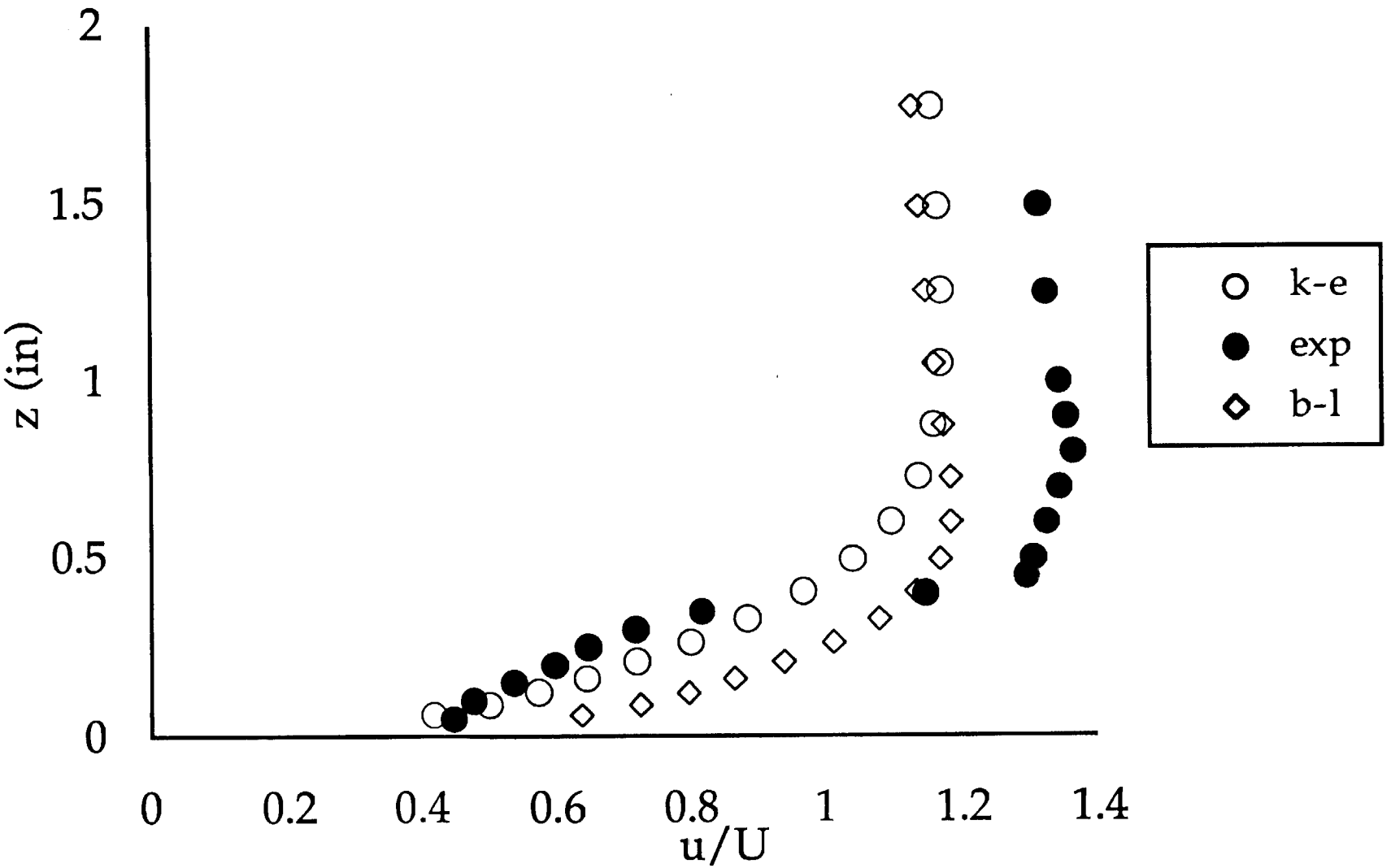

A Hybrid Navier-Stokes/Full-Potential Method for the Prediction of Iced Wing Aerodynamics

O. A. F. Mello* , A. Bangalore* and L. N. Sankar§

School of Aerospace Engineering
Georgia Institute of Technology
Atlanta, Georgia 30332

An abstract submitted to the Aircraft Icing Session of the
AIAA 32nd Aerospace Sciences Meeting, Reno, NV, 1994

SUMMARY

A hybrid method for computing compressible viscous flows is presented. This method divides the computational domain into two zones. In the outer zone, the unsteady full-potential equation (FPE) is solved. In the inner zone, the Navier-Stokes equations are solved. The two zones are tightly coupled so that steady and unsteady flows may be efficiently solved. The resulting CPU times are less than 50% of the required for a full-blown Navier-Stokes analysis. Sample applications of the method to an unswept iced wing at 4^{o} angle of attack are presented. Surface pressures are in good agreement with the measurements obtained by Bragg et al. at the University of Illinois. The full paper will contain additional results for clean and iced swept wing configurations and will include surface pressure as well as velocity field comparisons.

INTRODUCTION

The increased need for aircraft to operate under adverse weather conditions has led to a growing effort in the performance evaluation of aircraft under icing conditions. Although the qualitative effects of icing have been well known to include lift decrease and drag increase with premature separation at the leading edge, there remains a need for reliable quantitative results in order to allow operation under icing conditions within an adequate safety margin.

---

* Graduate Research Assistant, School of Aerospace Engineering
§ Professor, School of Aerospace Engineering. Senior Member, AIAA

The large number of parameters involved in describing the shape of ice accretion and its evolution in time make it impractical and expensive to build up the needed quantitative results solely from wind-tunnel studies, hence accurate numerical methods are clearly needed for this purpose.

Current work in this area include the experimental efforts by Bragg et al.[1-3], and the Navier-Stokes computations by Potapczuk[4], Cebeci[5] and Sankar et al.[6-9]. In an ongoing research effort at Georgia Tech, a 3-D Navier-Stokes code has been successfully applied to iced wing configurations. While the Navier-Stokes analysis gives satisfactory results, it is CPU intensive. Since a typical iced wing performance would involve several parameters (α, M_∞, Re, planform, ice accretion shape), the full Navier-Stokes code will be time-consuming. On the other hand, panel and FPE methods cannot accurately predict the loss in performance due to icing, even when coupled with a boundary-layer analysis, due to the occurrence of premature leading-edge separation and reversed flow.

In order to improve the efficiency of Navier-Stokes computations, the present work was initiated. In this approach, a zonal Navier-Stokes/Full-Potential solver developed by Sankar et al.[10] and extended to rotors by Tsung and Sankar[11] is applied to an iced wing configuration.

The Full-Potential solver used in the outer zone solves the unsteady compressible FPE in strong conservation form using the artificial compressibility concept and employing a strongly implicit procedure[12]. The Navier-Stokes solver used in the inner zone is identical to the one used in the previous iced wing efforts at Georgia Tech[6-9].

Historically, coupling potential flow to viscous flow via boundary-layer analysis has proved troublesome at the separation point and the recirculation region. Since we are computing the full Navier-Stokes equations in time-dependent form in the inner region, the above difficulties associated with boundary-layer methods are avoided.

The remaining of this abstract is organized as follows: First, the mathematical formulation of the Full-Potential and Navier-Stokes solvers are briefly given. Next, some sample applications of this method to the iced wing configuration tested by Bragg et al.[1,2] are

given. The abstract concludes with a list of additional results to be presented in the full paper.

MATHEMATICAL FORMULATION

Full-Potential Formulation

The 3-D unsteady compressible potential flow equation, in a body-fitted coordinate system, may be written in a strong conservation form as:

$$\left(\frac{\rho}{J}\right)_\tau + \left(\frac{\rho U}{J}\right)_\xi + \left(\frac{\rho V}{J}\right)_\eta + \left(\frac{\rho W}{J}\right)_\zeta = 0 \qquad (1)$$

where ρ is density and U, V and W are the contravariant components of velocity.

Using the isentropic gas law and the energy equation, equation (1) may be written[12] as a second order hyperbolic partial differential equation for ϕ:

$$\frac{\rho}{a^2 J}\left[\phi_{\tau\tau} + U\phi_{\xi\tau} + V\phi_{\eta\tau} + W\phi_{\zeta\tau}\right] = \left(\frac{\rho U}{J}\right)_\xi + \left(\frac{\rho V}{J}\right)_\eta + \left(\frac{\rho W}{J}\right)_\zeta \qquad (2)$$

At each point on the grid, the spatial derivatives are written using standard central difference formulas, which result in formal second-order accuracy in space.

Because equation (2) is hyperbolic, it may be advanced in time using a stable marching scheme. Here, a strongly implicit procedure is used. To circumvent the nonlinearities, the coefficients ρ , a^2, J , U , V and W appearing on the left side, and the density ρ appearing on the right side of equation (2) are computed at the time level 'n'. The remaining quantities in (2) are kept at the new time level 'n+1'.

The time derivatives and the mixed time and space derivatives appearing on the left side of (2) are approximated using first order accurate finite difference formulas such as:

$$\phi_{\tau\tau} \cong \frac{\phi^{n+1} - 2\phi^n + \phi^{n-1}}{\Delta t^2} \qquad (3a)$$

$$\phi_{\xi\tau} \approx \frac{\phi_i^{n+1} - \phi_{i-1}^{n+1} - \phi_i^n + \phi_{i-1}^n}{\Delta t \Delta \xi} \tag{3b}$$

When the above discretizations are employed, at each time step a system of linear equations result for the quantity $\Delta\phi = \phi^{n+1} - \phi^n$. This system of equations may formally be written in the form:

$$[M] \{ \Delta\phi \} = \{R\} \tag{4}$$

The matrix M is a sparse matrix with twenty seven diagonals, reflecting the fact that a node (i,j,k) is linked to its 26 neighbors. On nearly orthogonal grids such as the one used in the present work, only diagonals coupling (i,j,k) to its six neighbors (i+1,j,k) , (i-1,j,k), (i,j-1,k), (i,j+1,k), (i,j,k-1) and (i,j,k+1) are significant, and one may neglect the other cross-coupling terms, which results in a seven-diagonal matrix. This seven-diagonal system is then recast into the LU form using a strongly implicit procedure.

Navier-Stokes Formulation

The vector form of the full Reynolds-averaged, 3-D Navier-Stokes equations based on an arbitrary curvilinear coordinate system can be written as:

$$Q_\tau + (E - E_V)_\xi + (F - F_V)_\eta + (G - G_V)_\zeta = 0 \tag{5}$$

where Q is the vector of unknown flow properties; E, F, G are the inviscid flux vectors; and E_V, F_V, G_V are the viscous flux vectors.

The time derivative, Q_τ, of equation (5) is approximated using two-point backward difference at the new time level:

$$Q_\tau = \frac{(Q^{n+1} - Q^n)}{\Delta\tau} \tag{6}$$

where 'n' refers to the time level at which all quantities are known, and 'n+1' is the new time level. All spatial derivatives are approximated by standard second-order central differences and are represented by the differencing operators δ, e.g. $E_\xi \approx \delta_\xi E$.

The spanwise derivative, F_η, is evaluated explicitly at the old time level 'n', but uses the 'n+1' values as soon as they become

available. This semi-explicit treatment of the spanwise derivative enables the scheme to solve implicitly for all points at one spanwise station at a time. To eliminate any dependency the solution may have on the marching direction, the solver reverses the direction of marching with every spanwise sweep.

The viscous terms E_v, F_v and G_v are evaluated explicitly, using half-point central differencing, so that the computational stencil for the stress terms uses only three nodes in each of the three directions. Explicit treatment of the stress terms still permits the use of large time steps since the Reynolds numbers of interest here are fairly large.

The time and space discretizations described above lead to a system of non-linear, block penta-diagonal matrix equations for the unknown Q^{n+1}. The equation is then linearized using the Jacobian matrices $A = \partial E/\partial Q$ and $B = \partial G/\partial Q$ and approximately factored into a product of two block tri-diagonal matrix equations:

$$\begin{aligned}[I + \Delta\tau\, \delta_\xi A]\, [I + \Delta\tau\, \delta_\zeta B]\, \Delta Q &= R \\ = -\Delta\tau\, [\, \delta_\xi (E - E_v) + \delta_\eta (F - F_v) + \delta_\zeta (G - G_v)\,]\end{aligned} \qquad (7)$$

The use of standard central differences to approximate the spatial derivatives can give rise to the growth of high frequency errors in the numerical solution with time. To control this growth, a set of 2nd/4th order non-linear, spectral radius based, explicit artificial dissipation terms are added to the discretized equations. A second order implicit dissipation is used to help the overall numerical stability of the scheme.

A slightly modified version of the Baldwin-Lomax (B-L) algebraic turbulence model is used, where the maximum normal shear value is used instead of the wall shear stress because in the vicinity of separation points, the shear stress values approach zero at the wall.

Navier-Stokes/Full Potential Coupling

A typical partitioning of the domain into an inner zone and an outer zone is illustrated in Fig. 1. The plane $k=k_{MATCH}$ corresponds to the interface between the inner zone and the outer zone. The Navier-

Stokes solver is applied to all planes up to $k=k_{MATCH}$. The FPE solver is applied between the planes $k=k_{MATCH}$ -1 and the outer boundary k-plane. Therefore, the two zones actually overlap, which allows specification of boundary conditions at the interface without extrapolation.

RESULTS AND DISCUSSION

The hybrid Navier-Stokes/Full-Potential Method has been applied to an iced unswept wing configuration, which has been experimentally studied by Bragg et al.[1-3]. The surface pressures were measured at five spanwise stations: 17%, 34%, 50%, 66% and 85%.

The computational grid used in the present study was an algebraic C-grid with 141 × 19 × 41 grid points, with 121 points over the airfoil surface at each spanwise station. 14 spanwise stations were used along the wing, with 5 stations extending beyond the tip. The Navier-Stokes and Full-Potential solvers were interfaced at k_{MATCH}=21. The Mach number was 0.12, the Reynolds number 1.7321 million, and the angle of attack was 4°. The CPU time for this configuration was about 24 sec. per iteration on a Hewlett-Packard Apollo 700 workstation. The CPU time for the same configuration on Georgia Tech's Cray Y-MP/E was about 9.6 sec. per iteration. These times are about 50% of the times required for a full Navier-Stokes analysis. Computations were performed up to 1000 iterations, when the maximum residual and corrections were of order 10^{-5}.

The computed surface pressure distributions were linearly interpolated to allow comparisons at the spanwise stations where experimental data are available[1,2]. The resulting correlations are shown in Fig. 2. A good agreement may be observed between the numerical and experimental results, especially inboard, where the suction peaks behind the ice accretion can be clearly observed, although the sharp variations are somewhat displaced with respect to the experimental data. Less agreement is found towards the tip region, probably due to the three-dimensional character of the flow in this region, which would require a finer grid resolution near the tip. There are also spurious peaks near the trailing edge at all the spanwise stations, indicating that the grid resolution is not adequate there.

Overall, it is observed that our current results are basically identical to those obtained by a full Navier-Stokes code[6-9], while consuming only about 50% of the CPU time.

ADDITIONAL RESULTS TO BE FOUND IN THE FULL PAPER

The final paper will include additional results for clean and iced wing configuration, including surface pressure data and correlation of velocity profiles with LDV flowfield measurements obtained by Bragg et al.[3] for both unswept and swept wing configurations. We will also address in more detail further developments of this hybrid Navier-Stokes/Full-Potential method.

REFERENCES

1. Bragg, M. B., and Khodadoust, A., "Effect of Simulated Glaze Ice on a Rectangular Wing," AIAA Paper 89-0750, January 1989.

2. Khodadoust, A., and Bragg, M. B., "Measured Aerodynamic Performance of a Swept Wing with a Simulated Ice Accretion," AIAA Paper 90-0490, January 1990.

3. Bragg, M. B., Kerho, M. F., and Khodadoust, A., "LDV Flowfield Measurements on a Straight and Swept Wing with a Simulated Ice Accretion," AIAA Paper 93-0300, January 1993.

4. Potapczuk, M. G., "Numerical Analysis of a NACA 0012 Airfoil with Leading Edge Ice Accretions," AIAA Paper 87-0101, January 1987.

5. Cebeci, T., "Effects of Environmentally Imposed Roughness on Airfoil Performance," NASA CR-179639, June 1987.

6. Kwon, O. J., and Sankar, L. N., "Numerical Study of the Effect of Icing on Finite Wing Aerodynamics," AIAA Paper 90-0757, January 1990.

7. Kwon, O. J., and Sankar, L. N., "Numerical Study of the Effect of Icing on Fixed and Rotary Wing Performance," AIAA Paper 91-0662, January 1991.

8. Kwon, O. J., and Sankar, L. N., "Numerical Investigation of Performance Degradation of Wings and Rotors Due to Icing," AIAA Paper 92-0412, January 1992.

9. Sankar, L. N., Phaengsook, N., and Bangalore, A., "Effects of Icing on the Aerodynamic Performance of High Lift Airfoils," AIAA Paper 93-0026, January 1993.

10. Sankar, L. N., Bharadvaj, B. K. , and Tsung, F.-L., A Three-Dimensional Navier-Stokes/Full-Potential Coupled Analysis for Viscous Transonic Flow, AIAA Paper 91-1595-CP, presented at the AIAA 10th Computational Fluid Dynamics Conference, Honolulu, Hawaii, June 1991.

11. Tsung, F.-L., Ph.D. Dissertation (in preparation), 1993.

12. Sankar, L. N., Malone, J. B., and Tassa, Y., "An Implicit Conservative Algorithm for Steady and Unsteady Three-Dimensional Transonic Potential Flows," AIAA Paper 81-1016, June 1981.

Figures:

Fig. 1: Partitioning of Computational Domain into Inner and Outer Zones.

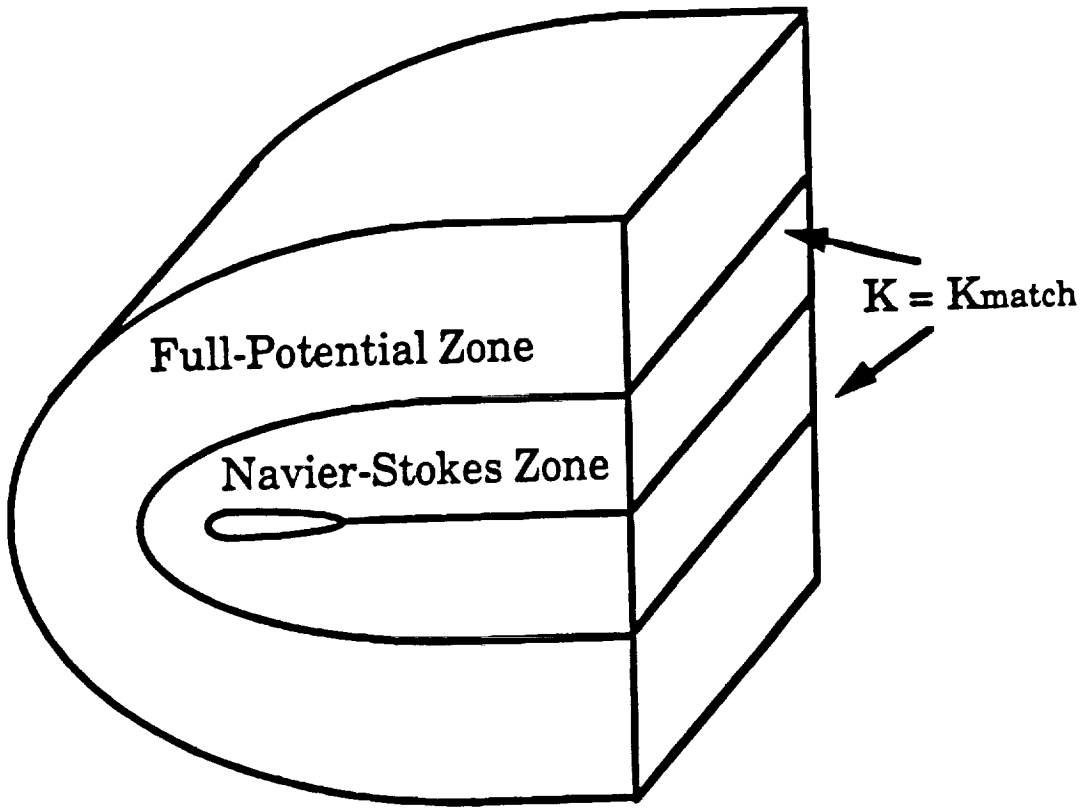

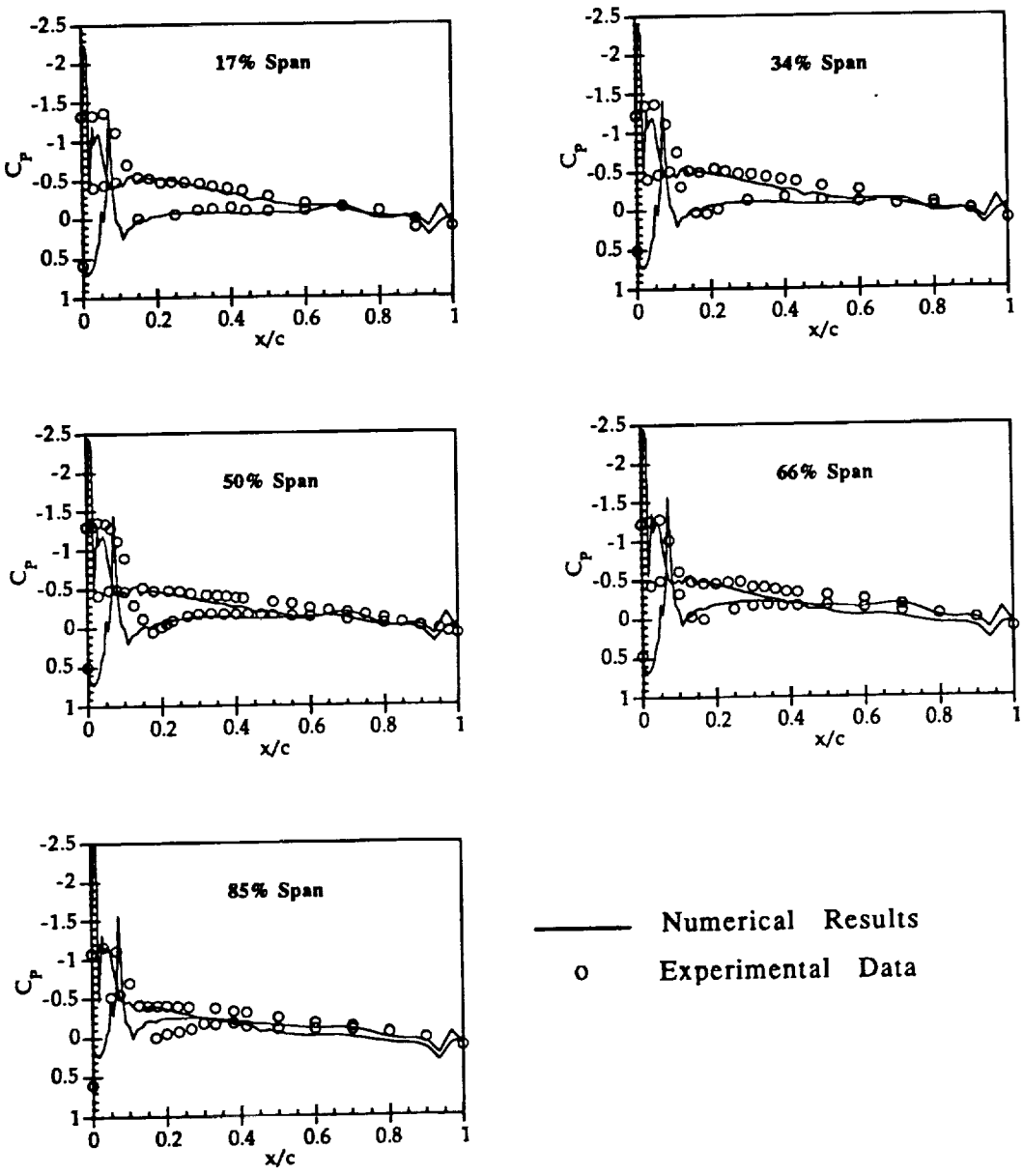

Fig. 2: Surface Pressure Distributions for Iced Unswept Wing at 4° Angle of Attack.